Fourth International Dam World Conference
PORTUGAL · LISBON · LNEC · September 21-25, 2020

DISPLACEMENT MONITORING IN CABRIL DAM USING GNSS




Miguel Rodrigues[1]	**Sérgio Oliveira**[2]	**José Nuno Lima**[3]	**Jorge Proença**[4]
Laboratório Nacional de Engenharia Civil	Laboratório Nacional de Engenharia Civil	Laboratório Nacional de Engenharia Civil	CERIS - Instituto Superior Técnico

ABSTRACT

The continuous displacement monitoring is essential for the safety control of large dams. It should be based on the comparison between numerical model results and monitoring data, *e.g.* observed displacements using plumb lines, geodetic methods or, more recently, with GNSS (Global Navigation Satellite System). For Cabril dam, the case study presented in this paper, no plumb lines were installed in the central section. Thus, the displacement monitoring in this section is carried out by classical geodetic methods that do not allow continuous monitoring (only two observation campaigns per year). So, in this case, the use of GNSS was considered particularly useful, as it allows continuous monitoring of displacements at the top of the central section. As Cabril dam presents cracking problems since the first filling, it is important to continuously monitor several notable points, which includes the point at the top of the central section. The present work focuses on the validation of the displacements obtained by GNSS, at Cabril dam, using a 3D finite element model, developed in MATLAB, in which the horizontal cracking at the upper zone is simulated through joint elements. The 3DFE model was calibrated based on the displacements observed by plumb lines (in two non-central sections) and by classical geodetic methods, considering variations in hydrostatic pressure and annual temperature variations. The displacement evolution observed by plumb lines and geodetic methods were analyzed using HSCT (Hydrostatic, Seasonal, Creep and other Time effects) separation of effects models, to facilitate the comparison process between the observed displacements and the numerical results. In this way, the 3DFE model was firstly calibrated using plumb lines results and then it was used to validate GNSS measurements.

Keywords: Arch dam, Monitoring, Safety control, Global Navigation Satellite System, Measuring displacements, HSCT model, 3D FEM.

[1]mrodrigues@lnec.pt, Portugal
[2]soliveira@lnec.pt, Portugal
[3]jnplima@lnec.pt, Portugal
[4]jorge.m.proenca@tecnico.ulisboa.pt, Portugal

1. INTRODUCTION

Large concrete dams are high potential risk structures whose safety control requires continuous monitoring. The safety control, in most dams, comprehends the displacement evolution analysis of some notable points. At the Cabril dam, the displacements in the upper central zone are only measured biannually with geodetic methods. Due to the dam curvature it was not possible to install plumb lines to measure that specific zone's displacements, reason why it was decided to install a GNSS system to measure displacements in that location. The GNSS system was installed in Cabril dam, Fig.1) in 2016 by LNEC and EDP as part of a project financed by FCT. The decision to install this system was also influenced by the fact that Cabril dam presents important horizontal cracking near the crest, which was detected during the first filling and occurred because the dam thickness increases near de crest what causes vertical tensions at the downstream face due to hydrostatic pressure for high reservoir levels. It was also identified at the upper inspection galleries gel exudations indicative of swelling reactions.

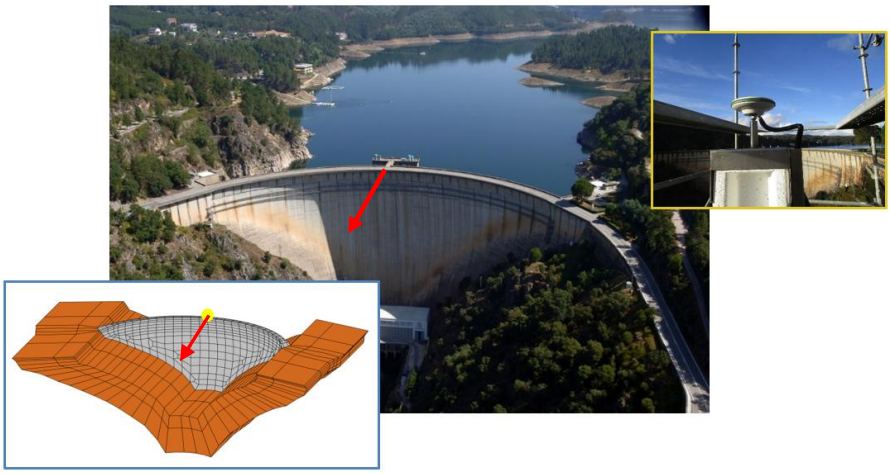

Fig. 1 – Cabril dam. GNSS antenna location at the top of central cantilever and 3DFEM discretization

2. USE OF GNSS FOR DISPLACEMENT MONITORING IN ARCH DAMS

The Global Navigation Satellite System (GNSS) allows to instantly determine the position and velocity of an observer, accurately and at a low cost, anywhere on Earth's surface. This explains why GNSS is the most used navigation system.

The main purpose of navigation is to determine the position and speed of a given point in a well-defined coordinate reference. Tests carried out on LNEC campus confirmed that using the same equipment 24 hours a day and under any weather conditions, GNSS was able to measure small-amplitude movements, either low-frequency or high-frequency [1]. Although

these characteristics make GNSS use possible in a wide range of applications, GNSS observation in dams aims to measure, in strategic points, the three displacement components, usually of small amplitude and exhibiting slow variations (low frequency variations). The permanent displacement observation with GNSS of notable points is an important contribution to the monitoring of dams structural response over time.

This type of monitoring requires a GNSS station installed at the dam points to be monitored and, at least, one more GNSS station located outside the dam, but near it, at a suitable location (fixed station), which is designated as the reference station, in order to allow the use of GNSS in relative mode - the most accurate mode. This method allows the measurement of the coordinate difference between a station positioned in the dam structure and the reference station located outside the dam (Fig. 2), this distance is called "base" or "vector". If one of the stations, being the reference station, is fixed, the permanent base measurement allows the horizontal component of the second GNSS station to be directly measured (located at the object point).

Fig. 2 – GNSS system installed in Cabril dam for measure the displacement at the top of central section

3. CABRIL DAM AND GNSS SYSTEM

Cabril dam is located on the Zêzere river and has been in operation since 1954. It is the highest arch dam in Portugal with a maximum height above the foundation of 132 m, with the crest at 297 m of elevation and a crest length of about 290 m. Cabril dam is a double curvature arch dam on a granite mass rock foundation.

A GNSS system, financed by FCT, was installed in Cabril dam by LNEC and EDP in 2016, to enable the continuous automatic measurement of the three displacement components at the top of the central section [2], with a sampling frequency of 20 Hz. This system includes a GNSS receiver located at a point outside the dam (about 200 meters afar from it), which is

being used as reference, and another GNSS receiver that was installed at the crest centre, the object point (Fig. 2). The location of the reference receiver favours error reduction because it has been installed in a stable location, with a free horizon, at the left bank. This system has been in operation since July 2016, continuously providing data, 24 values per day, allowing a better evaluation of Cabril dam's behaviour.

The Cabril dam's GNSS observations used in this study corresponded to the daily averages measured. This solution presents a much lower noise than, for example, the hourly averages solution, because the daily displacement variation of the pillar that supports the reference antenna, caused by the daily thermal variation, is eliminated when using the daily averages.

3.1. Plumb line and geodetic markings location

Considering that the calibration of the FE model will be based on comparisons between numerical results and observed displacements measured with plumb lines and using the triangulation method, the location of coordinometer bases and geodetic marks is shown in Fig. 3.

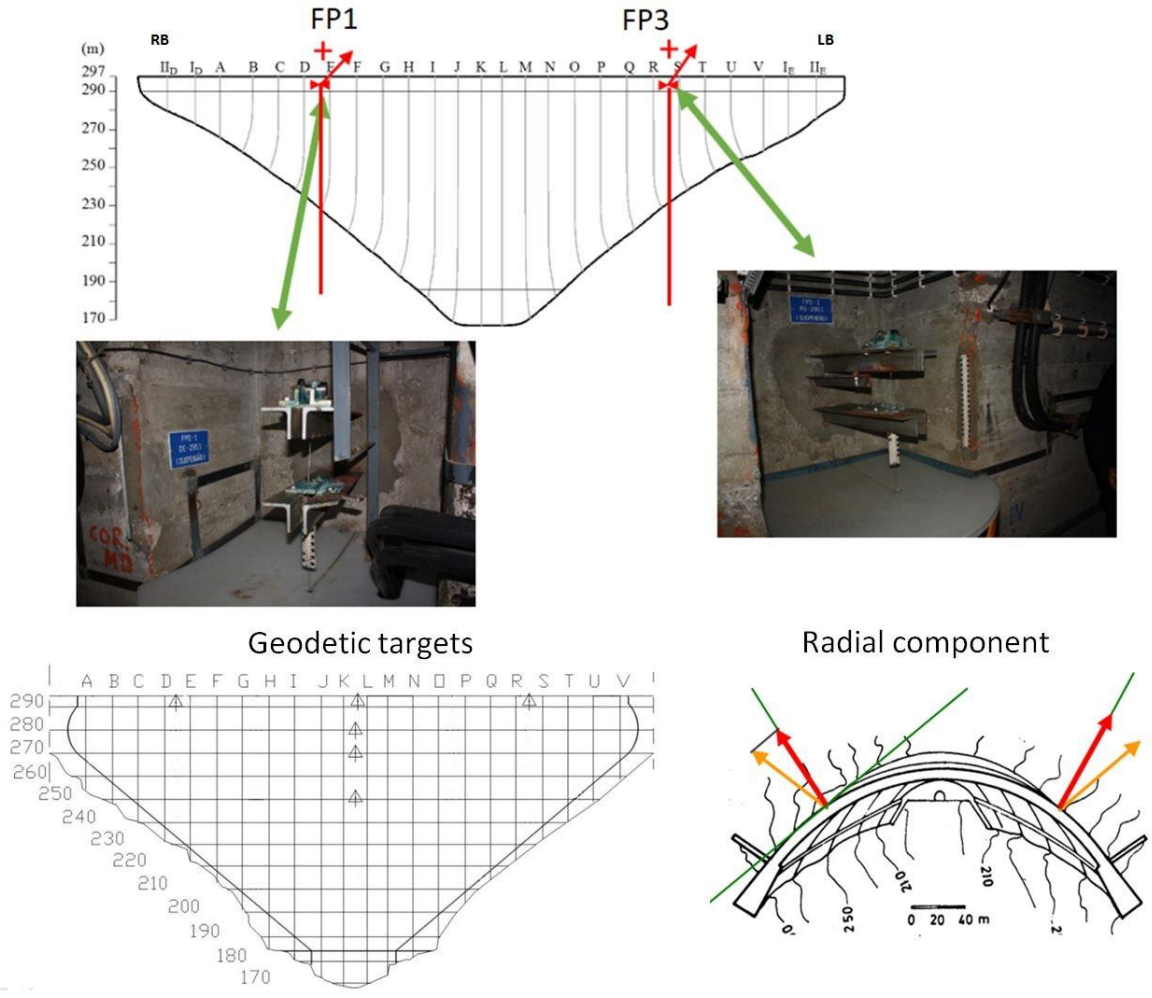

Fig. 3 – Plumb lines and geodetic marks used in the calibration of the 3DFE model

The plumb lines used for the Finite Element Model (FEM) calibration are FP1 and FP3 which are located at blocks DE and RS respectively as shown in Fig. 3. As for the geodetic marks used to aid the calibration of the FEM, they lie not only along the central block (KL) but also along two marks placed slightly below the bases of the FP1 and FP3 plumb lines. The results presented in this paper show the calibration of the FEM based on comparisons made between its results and the displacements observed at the coordinometer bases located at the top of FP1 and FP2, and at the geodetic mark located at the top of the KL block (near the location where the GNSS antenna was installed to measure displacements occurring at the top of the centre cantilever).

4. 3D FINITE ELEMENT MODEL

For Cabril dam structural behaviour analysis was developed a 3D finite element model using cubic FE (isoparametric, with 20 nodes) involving the dam and the foundation (Fig. 4). Hence, a discretization with three elements along the thickness was assumed for the dam body, which was automatically generated using the program Dam3DMesh1.0. This discretization considered that the existing horizontal cracking could be simulated using horizontal interface elements on the dam upper zone, as represented in Fig. 4 by the red band. This crack is considered closed on the upstream face and completely open in the entire thickness up to the downstream face. Fig. 4 shows the 3D mesh geometry and the material properties considered. It is relevant to note that this model geometry and its material definition is a result of continuous improvement by systematic comparison with observed data.

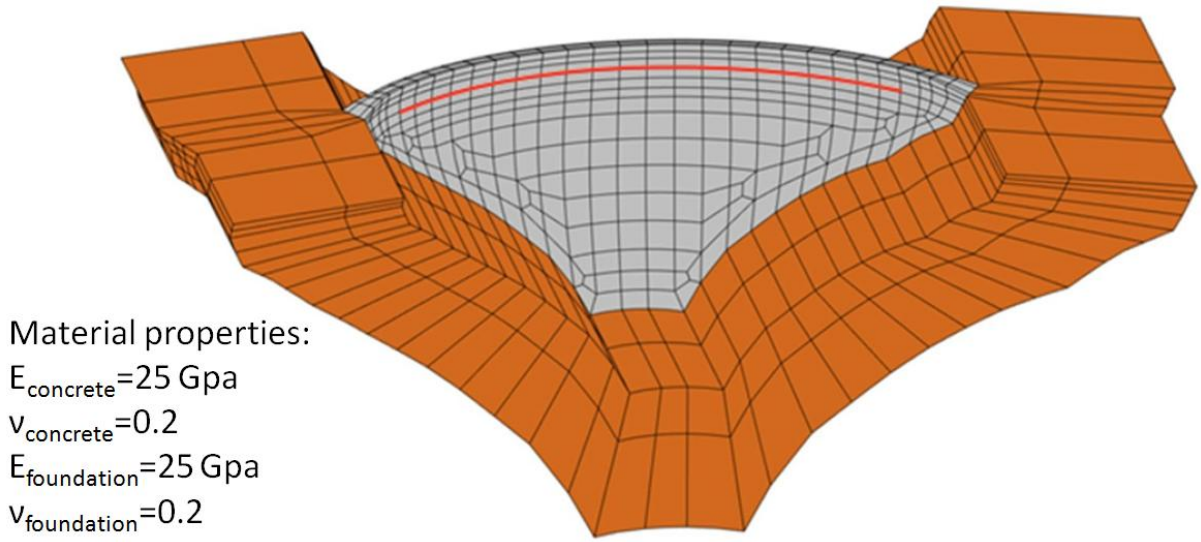

Fig. 4 – 3DFEM mesh generated automatically by Dam3DMesh1.0

5. USING THE PROGRAM DAMSAFE3.0

The dam structural analysis was performed by DamSafe3.0, a program developed in MATLAB which is used to carry out the dam's static analysis due to variations in temperature and water level. This program includes two modules: FEM and HSCT. The FEM module performs structural calculations based on the finite element method [3], and the HSCT module analyzes observed displacement histories using HSCT type separation of effects models.

5.1. FEM Module: DamSafe3.0

For the load combination SW+HP295, with Self-Weight (SW), and Hydrostatic Pressure (HP) for water level 295 m, the maximum displacements appears over the cracking area, with a value in the order of 43 mm, towards downstream, as can be observed in the deformed mesh (Fig. 5a).

Regarding the principal stresses for this load combination SW+HP295, Fig. 5b shows that, in the upstream face, the maximum compression stress is about -5.7 MPa at the upper centre zone and the maximum tensile stresses are about 2.85 MPa, in the dam heel. In the downstream face (Fig. 5c), the maximum compression stresses are of about 7.65 MPa and occur at the arches abutments.

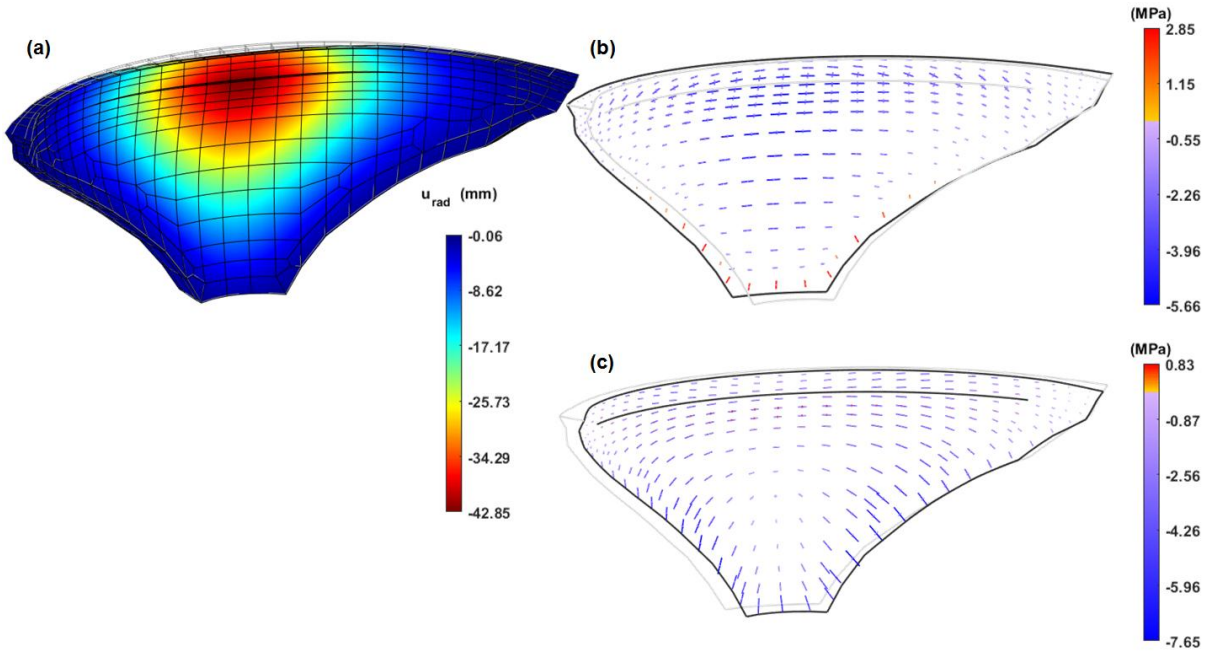

Fig. 5 – Dam response for the load combination: SW+HP295. (a) Radial displacements; (b) Principal stresses at the upstream face; (c) Principal stresses at the downstream face

5.2. HSCT Module. Separation of effects models

The effects separation models main purpose is to isolate the effect of each load, which facilitates the study of the influence of each load on the observed displacement histories and, in particular, facilitates the detection of any anomalous or pathological component of the observed displacement.

Among the pathologies of dams that can develop over time, swelling is becoming more relevant, arousing interest in its evolution and subsequent study of its effects. Many concrete dams have registered problems related to swelling due to chemical reactions occurring between cement components and the aggregate, namely alkali-silica reactions (alkalis present in the cement and silica in the aggregate) [4-7]. The swelling reactions occur with relatively high humidity and temperature, producing a gel that fills the concrete internal microstructure pores. This process eventually generates cracking, the consequent concrete damage, and a global volume increase (swelling). Many dams have problems due to swelling reactions, the most serious cases in Portugal are: Santa Luzia, Pracana and Alto Ceira. The case of Alto Ceira dam was an extreme example of concrete swelling pathological effect consequences, which led to the dam decommissioning. A new dam was constructed, Alto Ceira II dam, immediately downstream, that is now in full operation.

The HSCT-FEM model adopted in **DamSafe3.0**, allows the integrated use of FEM and HSCT models. In the analysis of the observed displacements histories, the HSCT models are able to separate the creep structural effect [8-10] (is assumed that the time effect in the foundation can be neglected) from the other time effects [11], using the next regression model (see table 1)

$$u\left(h,T_{\text{air}},t\right)=u_{\text{e}}^{\text{HP}}\left(h\right)+u_{\text{e}}^{\text{T}}\left(T_{\text{air}}\right)+u_{\text{C}}^{\text{HP}}\left(h,t\right)+u_{\text{C}}^{\text{SW}}\left(t\right)+u_{\text{swelling}}\left(t\right)+k \quad (1)$$

This HSCT model is capable of making the time effect separation into one creep component related to the hydrostatic pressure ($u_{\text{C}}^{\text{HP}}\left(h,t\right)$HP), one creep component associated with the self-weight ($u_{\text{C}}^{\text{SW}}\left(t\right)$), and one other time effects component (for example, swelling ($u_{\text{swe}}\left(t\right)$), foundation movements, *etc*.). In order to simulate the creep effect it is important to distinguish self-weight creep from hydrostatic pressure creep: for this purpose is useful to estimate the elastic response component for both loads. This procedure can be executed by the FEM.

The functions used to represent each separated effect correspondent to each term of the regression equation (Equation 1) are presented in Table 1.

Table 1 displays the use of exponential functions to represent the HP elastic effect. It should be noticed that FEM results can be used to better define the shape of the exponential function that characterizes the elastic response to the HP variation (in Fig. 7, as an example, on the top left graph is displayed a combination of exponential functions representing the HP elastic effect as computed by FEM).

The HP creep effect is obtained as a superposition response to a sequence of constant load steps (equivalent to a discretization of the water level variation in constant intervals): creep coefficients are applied to the elastic displacement values calculated for each constant water level interval. The viscoelastic response is equal to the superposition of the creep effect computed for each constant interval. The creep effect estimation for the water level variation is given by the following equation

$$u_{\mathrm{C}}^{\mathrm{HP}}(h,t) = a \times \left[\sum_{j=1}^{p} \phi\left(t, t_j^{'}\right) \left(e^{h_j / c_{\mathrm{f}}} - e^{h_{j-1} / c_{\mathrm{f}}} \right) - \sum_{j=1}^{p'} \phi\left(t_a, t_j^{'}\right) \left(e^{h_j / c_{\mathrm{f}}} - e^{h_{j-1} / c_{\mathrm{f}}} \right) \right] \quad (2)$$

Table 1 – Adjustment functions used for each term of the regression equation

Term	Effect	Adjustment function
$u_{\mathrm{e}}^{\mathrm{HP}}(h)$	Hydrostatic pressure elastic effect	$a\left(e^{h/c_{\mathrm{f}}} - 1\right)$, $15 \lesssim c_{\mathrm{f}} \lesssim 35$ (alternatively, the *a* value can be determined by the FEM)
$u_{\mathrm{e}}^{\mathrm{T}}(T_{\mathrm{air}})$	Temperature effect	bT_{air} or $b_1 \cos\left(\frac{2\pi \overline{t}}{365.25}\right) + b_2 \sin\left(\frac{2\pi \overline{t}}{365.25}\right)$, $\left(0 < \overline{t} < 365.25 \text{ days}\right)$ [12]
$u_{\mathrm{C}}^{\mathrm{HP}}(h,t)$	Hydrostatic pressure creep effect	$\sum \phi(t)\, \Delta u_{\mathrm{e}}^{\mathrm{HP}}$
$u_{\mathrm{C}}^{\mathrm{SW}}(t)$	Self-weight creep effect	$\phi(t) u_{\mathrm{e}}^{\mathrm{SW}}$
$u_{\mathrm{swelling}}(t)$	Swelling	$c \times \left(1 - e^{-t^n/\beta}\right)$ where $\beta = t_{\mathrm{hs}}^n \times n/(n-1)$, $n = 3.258$ and $t_{\mathrm{hs}}^n \simeq 8000$ days (hs – half swelling)
k	Independent term	-

Fig. 6a presents a theoretical example of a reservoir water level evolution over time and its discretization for the abovementioned calculus. Fig. 7 dark blue colour curve serves as an example of a typical HP creep effect evolution over time.

The temperature effect can be simulated with the air temperature values registered at the site (it is usual to apply a phase shift of approximately 20 to 30 days, which is roughly the dam response time to an air temperature variation) or by harmonic functions with annual

and/or half annual period [12]. Fig. 7 orange colour curve serves as an example of a typical temperature effect evolution over time.

The self-weight creep effect is a viscoelastic dam response to the self-weight (SW) load. The SW is a constant action following gravity's direction, applied to the whole structure, developing a creep effect that can be estimated by the elastic displacements predicted by the FEM for the SW, based in the creep coefficients estimated by the creep function and taking into account the structure concrete mean age from the end of the construction period.

Fig. 6b presents a theoretical example of the evolution over time of the two SW displacement components, with the grey colour is represented the creep displacement component, u_C (u_e is the SW elastic response determined by the FEM). Fig. 7 green colour curve serves as an example of a typical SW creep effect evolution over time.

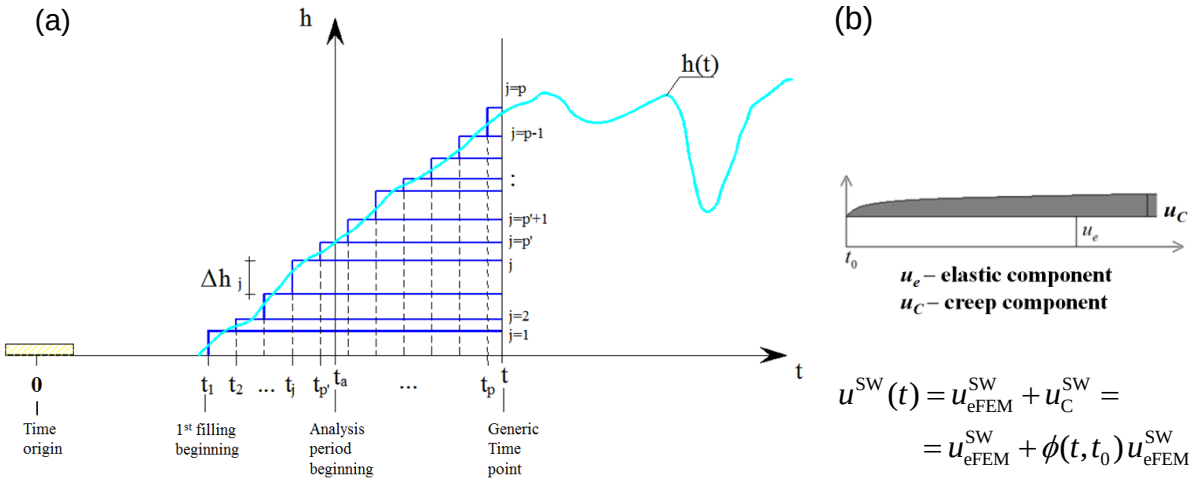

Fig. 6 – Creep behaviour over time (the reference campaign for time counting is approximately coincident with the mean construction period date). (a) Reservoir level discretization in even intervals; (b) SW elastic creep component

The adjustment function associated with the displacements created by the swelling effect is presented in Table 1 and an example of its development over time is presented in Fig. 7 by the red colour curve. The result is a sigmoid type curve, which slowly increases over time until half of its total displacement, where, at that point, changes from convex to concave (inflection point), moving then towards stabilization. The referred curve inflection, in what relates to swelling, is also named half-swelling point. Alternatively, the swelling effect can be represented by a polynomial function. The use of a polynomial or sigmoid type function depends on the one that better adjusts itself to the observed data.

The independent term, *k*, is included in the model so it can take into account the initial observation (the first campaign of the analysed period), *id est*, *k* contains the variability of the dependent variable (displacements) not explained by the independent variables (effects).

With this formulation, with the observation data, with a FEM model and with the resort to the Least Squares Method (LSM), a curve is obtained adjusted to the observations (for example, the grey colour curve in Fig. 7). It is important to point out that, before applying the LSM, the SW creep component is subtracted from the observed displacement values.

In order to obtain reliable results for the HSCT-FEM outputs is convenient to have observations in quantity, preferably obtained with assured quality and well distributed over time, where observed values are present at each year's seasons and at water levels representative of all the reservoir filling levels.

5.3. Applied HSCT-FEM model

This paper presents the measured displacement histories with the use of the plumb line, triangulation and GNSS methods.

Considering the methodology presented in the previous sub-chapter, after testing multiple regression model variations, the HSCT-FEM model which presented the best global adjustment, involving all observed dam points, had the following characteristics: (i) for the HP elastic effect estimation was considered one exponential function with a c_f value of 25 (although, it is important to note that for the analysis of the plumb lines was considered an additional exponential with c_f value of 20, because, at the analyzed locations, with the water level rise from empty reservoir to maximum capacity, there is not a monotonic increase in the measured displacements and, therefore, one exponential function alone cannot adjust itself correctly to the observable data, because of its monotonic nature; such result is easily observable in the top left graphs of Fig. 7 and Fig. 8; additionally, considering the plumb line points location near the embankments and the usual difficulty for the separation of effects models to adequately estimate the behaviour on those locations, the FEM results were used to draw the HP influence line); (ii) the temperature elastic effect is estimated by the observed daily average air temperature, considering an 18 days delay to simulate the heat wave propagation throughout the concrete; (iii) the HP creep effect is simulated by the creep coefficients application to the elastic response, for the monthly water level history discretization in constant intervals, and considering a concrete material with a Bazant and Panula creep law in which: E_0 = 41.5 GPa, ϕ_1 = 1.8, β = 0.05, m = 0.34 and n = 0.22, matching a concrete moderately damaged by swelling (there is evidence of swelling reaction occurrence, being visible, in open sight, gel exudations, at the upper inspection gallery); (iv)

the self-weight creep effect is estimated with the same creep coefficient application to the elastic displacements determined by the FEM, for the SW action; (v) the time effect related to swelling is given by a 3 terms polynomial, t^3+t^2+t. The resulting regression equation has the following form,

$$\begin{aligned} u-\phi(t,t_0)u_{\mathrm{e,FEM}}^{\mathrm{SW}} = {} & a_1.\left(e^{h/20}-1\right)+a_1.\sum\phi(t)u_{\mathrm{e},a_1}^{\mathrm{HP}}+ \\ & +a_2.\left(e^{h/25}-1\right)+a_2.\sum\phi(t)u_{\mathrm{e},a_2}^{\mathrm{HP}}+b.T_{\mathrm{air}}+c_1.t^3+c_2.t^2+c_3.t+k \end{aligned} \tag{3}$$

$$\sum\phi(t)u_{\mathrm{e},a_1}^{\mathrm{HP}} = \sum_{j=1}^{p}\phi\left(t,t_j^{'}\right)\left(e^{h_j/20}-e^{h_{j-1}/20}\right)-\sum_{j=1}^{p'}\phi\left(t_a,t_j^{'}\right)\left(e^{h_j/20}-e^{h_{j-1}/20}\right) \tag{4}$$

$$\sum\phi(t)u_{\mathrm{e},a_2}^{\mathrm{HP}} = \sum_{j=1}^{p}\phi\left(t,t_j^{'}\right)\left(e^{h_j/25}-e^{h_{j-1}/25}\right)-\sum_{j=1}^{p'}\phi\left(t_a,t_j^{'}\right)\left(e^{h_j/25}-e^{h_{j-1}/25}\right) \tag{5}$$

As mentioned, to apply HSCT-FEM hybrid models, FEM model results are necessary. As it is possible to verify in the previous paragraph and in equation 3, the FEM results are used for the estimation of the SW displacement component and for the estimation of the HP elastic effect at the plumb line coordinometer bases. These FEM results, like the HP elastic effect and the temperature effect, are also used to verify the agreement between the HSCT and the numerical model, as will the following figures display.

Considering the short analyzed period from the GNSS, it is assumed that no time effects are developed, therefore, those effects are not considered in the separation of effects model, only the temperature and HP effect are considered.

6. RESULTS

From Fig. 7 to Fig. 12 are presented the HSCT-FEM results for the radial displacements. This figures present the HSCT-FEM results along some notable dam points with the objective of ascertaining a good global agreement between the observed (HSCT model) and the simulated (FEM) and thereby validating both of them. Fig. 7 and Fig. 8 represent the radial displacements measured by the plumb line method at the coordinometer bases located near the crest, in blocks DE and RS respectively. The plumb line results are characterized by their good precision and spread over time, with measurements for every thermal season and every reservoir filling level. The plumb-lines symmetric location in relation to the dam centre axis (30 degrees to each side, from the dam arch centre) also help to understand if there is any asymmetric structural behaviour. Fig. 9 and Fig. 10 present the measurement results from the triangulation method. This method is characterized by its low measurement frequency, but since its displaying results at the dam centre axis, near the crest, at

approximately the same location of the GNSS antenna, which is the objective of this study, its results are important. Finally, Fig. 11 presents the GNSS radial displacement results of nearly three years of measurements. Its agreement with the global dam behaviour, in general, and in particular, with the geodetic marks located near its location and with the FEM calibrated results at the GNSS antenna location, show its usefulness in dam observation. In Fig. 12 is presented a simpler separation of effects of the triangulation observations at the geodetic mark at the top of the central section for direct comparison with the GNSS results. Considering the objective in question, it was only taken into account the HP and the temperature effects, and the analyzed period is similar to the one available by the GNSS.

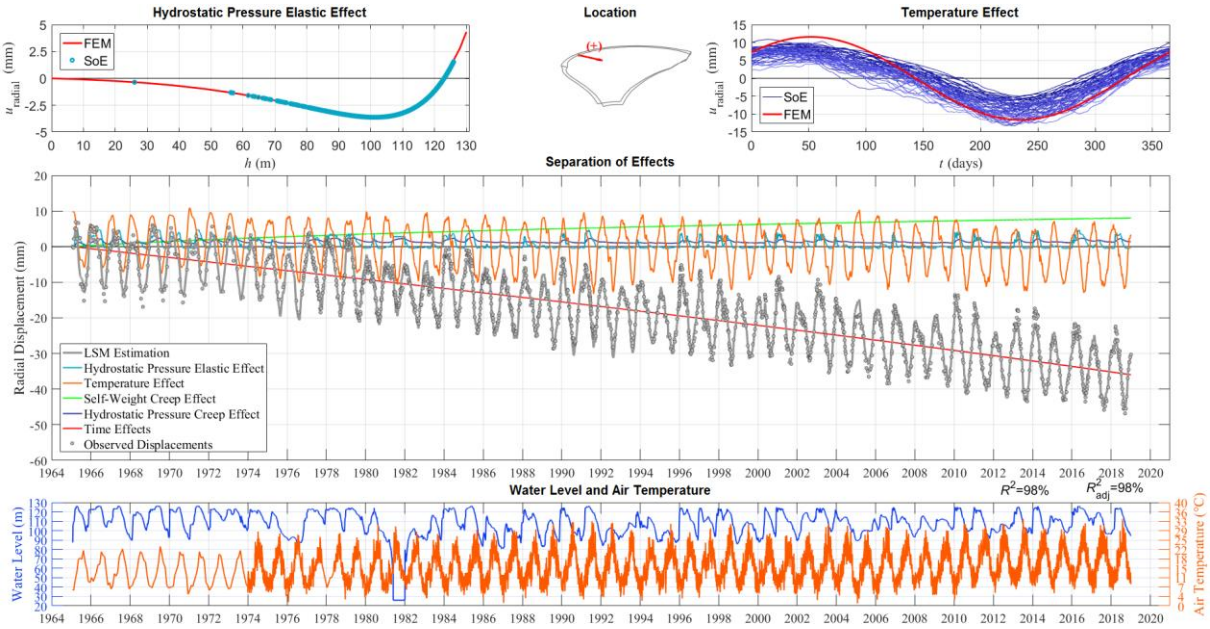

Fig. 7 – HSCT separation of effects results for the radial displacements measured by the plumb line method at coordinometer base FDE1 (elevation 294.6 m)

From the analysis of Fig. 7 to Fig. 11, as a whole, is possible to observe, in the main separation of effects graph (the central one in each figure), that there is a good agreement between the LSM curve (grey curve) and the observations from each instrument (grey dots), furthermore, this conclusion is supported by the high coefficients of determination obtained, greater than 96%, for these analyzed cases.

It is also important to note that, in Fig. 9 to Fig. 11, from the analysis of the HP elastic effect and temperature effect graphs (the top two in each figure) of the same group of figures, that all of them present a good agreement between what was estimated by the HSCT statistic model (blue dots for the HP elastic effect graph and blue curves for the temperature effect graph) and the FEM numerical model (red curve on both graphs), where the differences between the results are not spread afar. This good agreement between these two models for both HP pressure effect and temperature effect verify the FEM model validity and, therefore,

these results also contribute to verify the GNSS radial displacement measurements validity, where the observed is coherent with the validated simulated results.

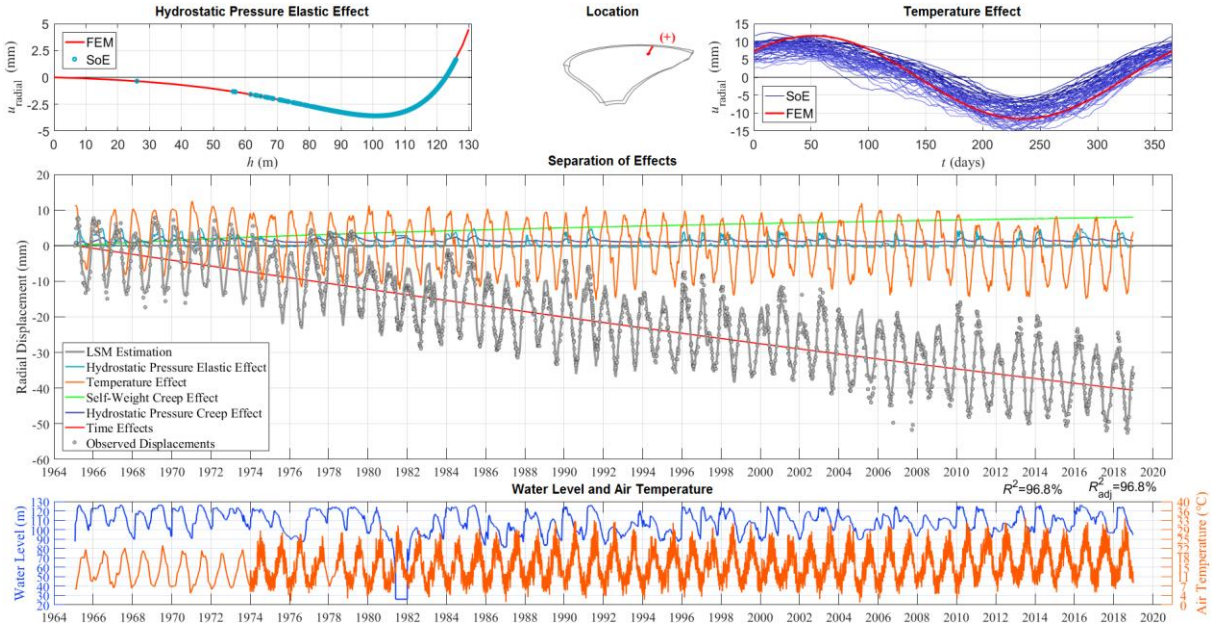

Fig. 8 – HSCT separation of effects results for the radial displacements measured by the plumb line method at coordinometer base FRS1 (elevation 294.6 m)

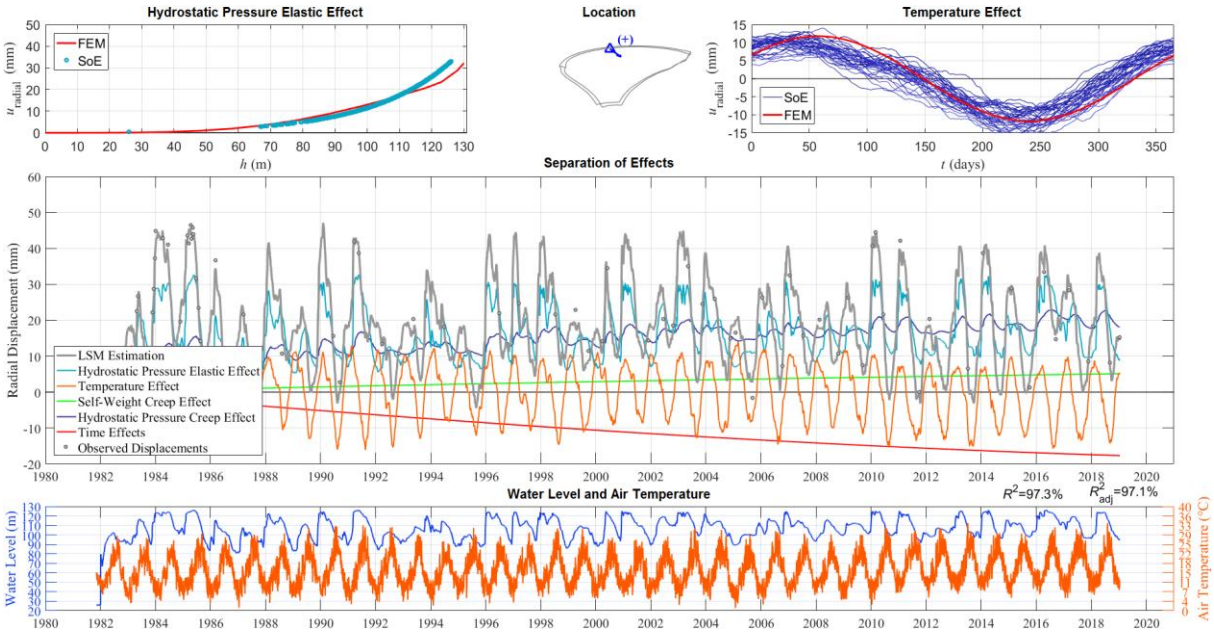

Fig. 9 – HSCT separation of effects results for the radial displacements measured by triangulation at the geodetic mark positioned in block KL at elevation 295 m

Naturally, in the above mentioned figures central separation of effects graph, over time, the HP elastic effect component follows the water level variation, as does the temperature effect follows the air temperature variation.

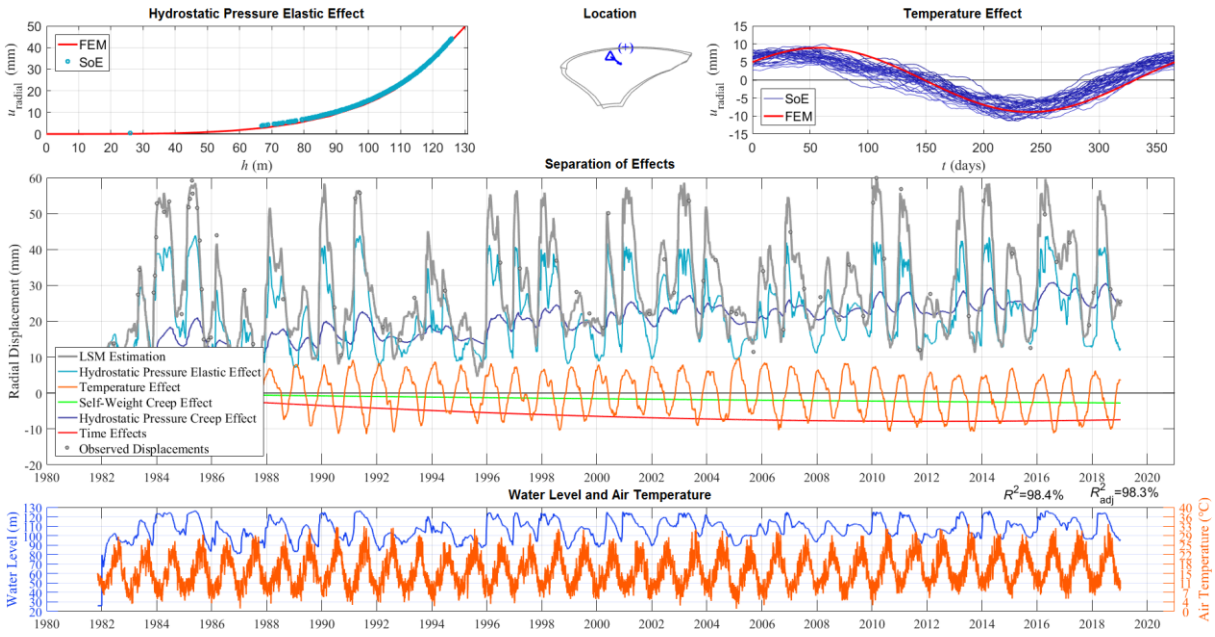

Fig. 10 – HSCT separation of effects results for the radial displacements measured by triangulation at the geodetic mark positioned in block KL at elevation 280 m

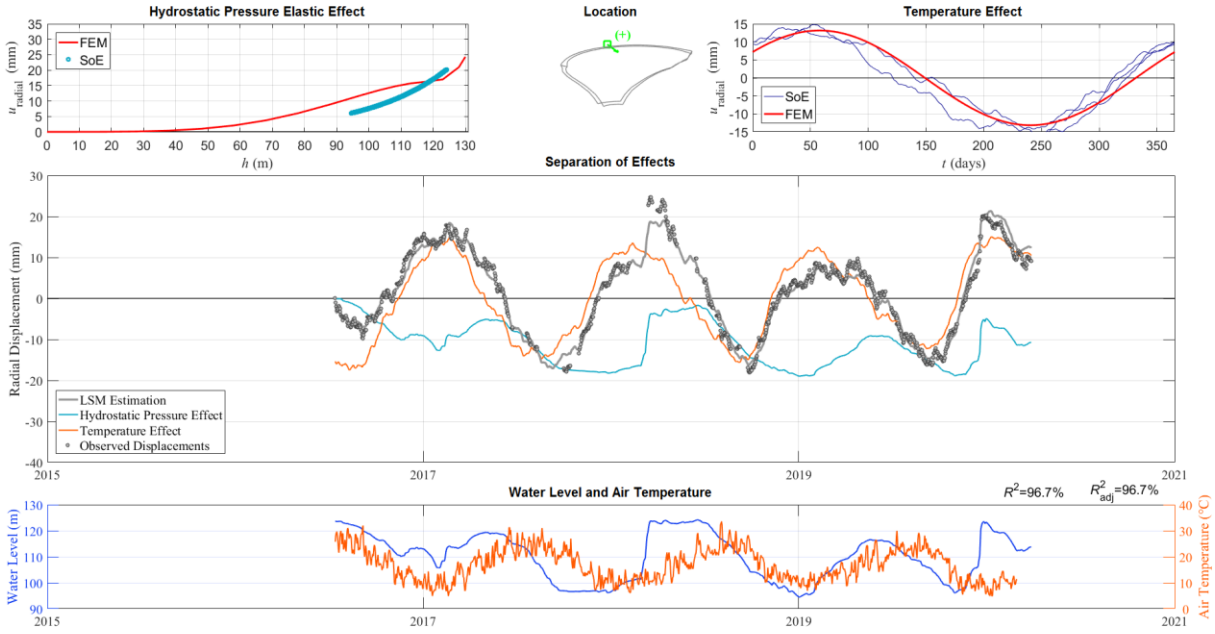

Fig. 11 – Separation of effects results for the radial displacements measured by GNSS at the antenna located in block KL at elevation 297 m

The top coordinometer bases separation of effects analysis (Fig. 7 and Fig. 8) point to an approximate symmetric structural behaviour, whether one considers the HP, the temperature or the time effects. Considering the time span of these analysis, they also demonstrate that the time and the SW creep effects are the most prominent effects, one towards upstream and the other opposing it, towards downstream, respectively. The time effect is probably mostly due to the swelling reactions effect, since gel exudations are visible in open sight at

the upper inspection gallery. Fig. 8 and Fig. 9 present the triangulation separation of effects results and, although the geodetic mark is located in a different position (over the dam centre axis, near the crest), it is also verifiable, even considering a smaller time span, that the same effects are the most prominent and with a similar evolution over time. Contrarily, in the GNSS separation of effects (Fig. 11), it is not possible to clearly discern a time effects component, nevertheless, the limited time span (almost three years of monitoring) is not enough to take a conclusion about the evolution of this effect.

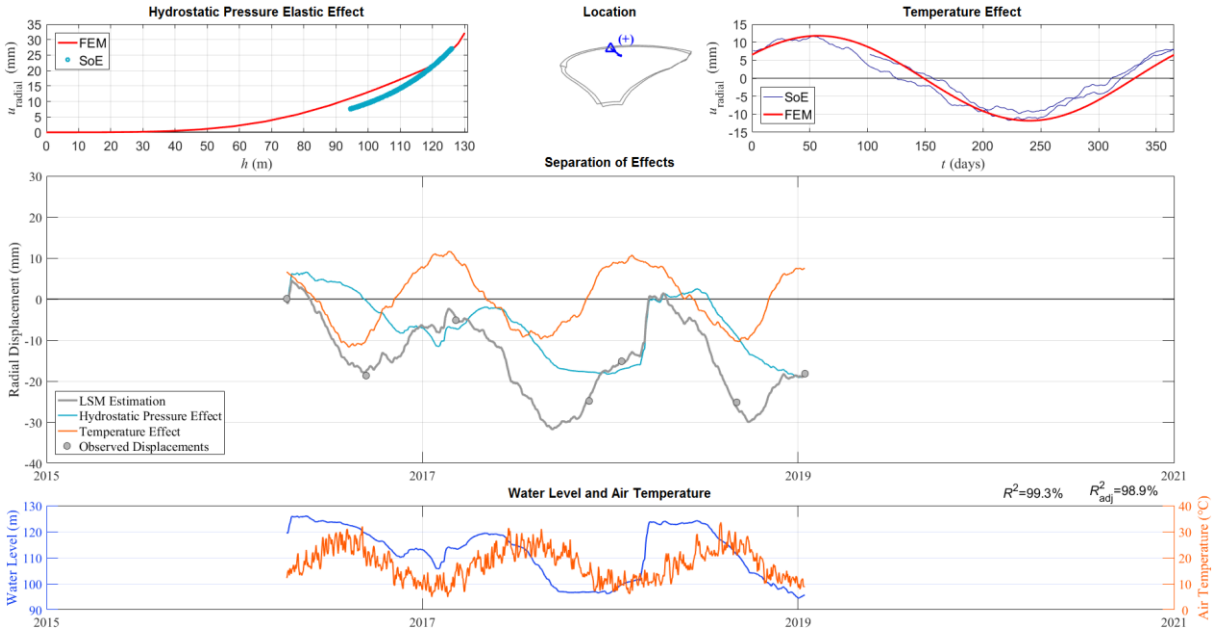

Fig. 12 – Separation of effects results for the radial displacements measured by triangulation at the geodetic mark positioned in block KL at elevation 295 m

Fig. 12 displays the separation of effects results for a model identical to the one used on the GNSS observation data analysis, considering an approximate analyzed period as well. Although, the observations from the triangulation method are much less in quantity than those provided from the GNSS for the same analyzed period, it is relevant to note the similarity between the LSM solution obtained and the equivalent solution obtained in the GNSS separation of effects (Fig.11), which once more is indicative of the GNSS method good reliability. Furthermore, this conclusion is supported by a great proximity between the LSM estimate and the triangulation observations.

7. CONCLUSIONS

In this paper it was analyzed the displacement history measured by GNSS at the antenna located in the top of central section of Cabril dam. The main objective was to verify the GNSS system reliability. Taking into account that at the crest centre it is not possible to measure displacements by the plumb line method, only by triangulation campaigns carried

out once or twice a year, it was decided that the best strategy to verify the reliability of the displacements measured by GNSS would be to validate a FEM using the abundant plumb line observations and then, with the validated FEM, verify if the GNSS observations were coherent.

The good fit between HSCT-FEM model and the radial observations measured by the plumb line, triangulation or even the GNSS method were all coherent with the FEM model applied in this study. Not only the overall adjustments presented a good fit, but the HP elastic effect and the temperature effect also presented a good adjustment to the applied FEM. The adopted FEM considered a crack fully open from the downstream face to the upstream face, which proved to be a better solution than the one adopted in a previous study [13], which considered, the same crack, open until 3/4 of the total length (the total length is equal to the dam thickness at that location), because the previous study considered higher displacements for the HP influence line, calculated by the FEM, which were incompatible with what now results from the GNSS separation of effects, considering nearly three years of monitoring, opposing the only 6 months of monitoring considered in the last study.

Hence, the good adjustment between the adopted FEM model and the HSCT-FEM results, for the coordinometer bases and triangulation marks analyzed, not only proves the good calibration of the applied FEM, but actually, the good quality of the separation of effects results obtained already by GNSS, with corresponding high coefficient of determination, helped towards adopting a better FEM model.

Naturally, the redundancy of instruments used in the FEM calibration granted its validity, thus, when comparing its results with those obtained by the HSCT-FEM separation of effects for the GNSS radial displacement measurements, the agreement was also very good, validating, as expected, the GNSS results.

The significant time effect component detected in every instrument data analysed (with the exception of the GNSS, because of its limited monitoring period), probably mostly due to the swelling reactions effect, should deserve further study due to its pathological nature.

Ultimately, the quality of the GNSS data analyzed enabled the initial goal of this study to be surpassed, because the GNSS data was not simply used for comparison with FEM model results for its validation, it was also used, due to its quality, to validate the FEM itself and contribute to the development of a better FEM. It is now more evident that the horizontal cracking at Cabril dam can be better simulated by the FEM when it considers a crack fully open. The GNSS clearly presents itself as an accurate, reliable and high frequency remote instrument to monitor dam displacements.

REFERENCES

[1] Lima, J. N. (2015). A utilização de filtros digitais em séries temporais GNSS. In: VIII Conferência Nacional de Cartografia E Geodesia. October 29 and 30th. Amadora, Portugal.

[2] Oliveira, S.; Lima, J. N.; Henriques, M. J. (2014). A Integração do GNSS no Controlo de Segurança de Grandes Estruturas. In: Jornadas Portuguesas de Engenharia de Estruturas (V). November 26 to the 28th. Lisbon.

[3] Zienkiewicz, O. C.; Cheung, Y. K. (1967). The Finite Element Method in Structural and Continuum Mechanics: Numerical Solution of Problems in Structural and Continuum Mechanics. McGraw-Hill.

[4] Silva, H. S. (1993). Estudo do envelhecimento das barragens de betão e de alvenaria. Alteração físico-química dos materiais, Specialist Thesis, LNEC.

[5] Gomes J. P. (2007). Modelação do comportamento estrutural de barragens de betão sujeitas a reações expasivas, PhD Thesis, FCT-UNL.

[6] Esposito, R.; Anaç, C.; Hendriks, M.; Çopuroğlu, O. (2016). Influence of the Alkali-Silica Reaction on Mechanical Degradation of Concrete. Journal of Materials in Civil Engineering 28(6).

[7] Abd-Elssamd, A.; Ma, Z. J.; Le Pape, Y.; Hayes, N. W.; Guimaraes, M. (2020). Effect of Alkali-Silica Reaction Expansion Rate and Confinement on Concrete Degradation. ACI Materials Journal Journal 117(1): pp. 265:278.

[8] Ramos M. (1985) Consideração da reologia do betão no comportamento de barragens, Specialist Thesis, LNEC.

[9] Ramos, M.; Pinho, J. (1987). A new method for quantitative analysis of dam displacements. In: III Int. Conf. on Computational Methods and Experimental Measurements. Oporto.

[10] Batista, A.; Ramos, J.; Oliveira, S.; Gomes, P. (2002). Models for safety control of concrete dams. In: 3rd International Conference on Dam Engineering: pp. 1:8. CI-Premier. Singapore.

[11] Oliveira, S. (2000). Modelos para análise do comportamento de barragens de betão considerando a fissuração e os efeitos do tempo. Formulações de dano, PhD Thesis, FEUP.

[12] Willm, G.; Beaujoint, N. (1967). Les méthodes de surveillance des barrages au service de la Production Hidraulique d'Electricité de France; Problèmes anciens e solutions nouvelles. In: IX ICOLD Congress, R.30, Q.34. Istanbul.

[13] Morais, R. (2017). Monitorização de deslocamentos em grandes barragens utilizando GNSS. Aplicação à barragem do Cabril, Master Thesis, ISEL.